

ORIGINAL RESEARCH

# FNDC5/PPAR $\alpha$ Pathway Alleviates THP-1-derived Macrophage Pyroptosis and Its Mechanism

Bo Zhou, MD; Guangjian Zhao, MM; Hui Li, MD; Quanwei Zhao, MM; Danan Liu, PhD

## ABSTRACT

**Context** • Atherosclerosis (AS) is a chronic inflammatory disease. Pyroptosis is a newly discovered, pro-inflammatory cell death that can trigger and amplify the occurrence and progression of AS. Researchers are still uncertain about the anti-atherosclerotic mechanism of “fibronectin type III domain-containing protein 5” (FNDC5).

**Objective** • The study aimed to investigate the ability of FNDC5-mediated, “peroxisome proliferator activated receptor alpha” (PPAR $\alpha$ ) to inhibit oxidized low-density lipoprotein (ox-LDL)-induced, THP-1-derived macrophage pyroptosis and to determine a potential molecular mechanism at the cellular level.

**Design** • The research team performed a laboratory study.

**Setting** • The study took place in the Department of Cardiovascular Medicine at the Affiliated Hospital of Guzhou Medical University at the Medical Research Institute at Guizhou Medical University in Guiyang, Guizhou, China.

**Outcome Measures** • The research team: (1) constructed and stably transfected FNDC5 gene-overexpressing and FNDC5 gene-silencing lentiviral vectors into THP-1 cells; (2) observed the cell morphology under an inverted fluorescence microscope and screened the stably transfected THP-1 cells with puromycin; (3) verified the transfection efficiency using quantitative real-time polymerase chain reaction (qRT-PCR) and Western Blot; (4) used phorbol to induce THP-1 cells into macrophages; (5) cultured the THP-1-derived macrophages with different concentrations of ox-LDL—25, 50, 75, and 100  $\mu\text{g/ml}$ —for 24 h; (6) performed Hoechst 33342/ propidium iodide (PI) double staining and examined lactate dehydrogenase (LDH) and interleukin-1 beta (IL-1 $\beta$ ) activity to determine the effects of ox-LDL on THP-1-derived macrophage pyroptosis; (7) selected the optimal ox-LDL concentration; (8) divided the THP-1-derived macrophages into seven groups: NC group (no ox-LDL intervention), ox-LDL group, PBS group, Mock1 group, Ad-FNDC5 group, Mock2 group, and Sh-FNDC5 group; (9) examined the expressions of

functional proteins and the pyroptosis of THP-1-derived macrophages, including FNDC5, PPAR $\alpha$ , and “nuclear factor kappa-light chain enhancer of activated B cells P65” (NF- $\kappa\text{B}$  P65), and those related to the pyroptosis pathway, using Western Blot and Hoechst 33342/PI double staining, respectively; (10) treated the THP-1-derived macrophages with FNDC5 expression with GW6471, a specific PPAR $\alpha$  antagonist; (11) determined the expressions of functional proteins and the pyroptosis of THP-1-derived macrophages, including FNDC5, PPAR $\alpha$ , and NF- $\kappa\text{B}$  P65, and those related to the pyroptosis pathway, using Western Blot and Hoechst 33342/PI double staining and detection of the LDH and IL-1 $\beta$  activity, respectively.

**Results** • With the stably transfected THP-1 cells with FNDC5 overexpression or silencing the ox-LDL-induced, THP-1-derived, macrophage pyroptosis occurred in a concentration-dependent manner. Compared with the ox-LDL, phosphate buffered saline (PBS), Mock1, and Mock2 groups, the Ad-FNDC5 group had a significant increase in expression of FNDC5 and of peroxisome proliferator activated receptor alpha (PPAR $\alpha$ ) proteins ( $P < .05$ ). The “nuclear factor kappa-light chain enhancer of activated B cells P65: (NF- $\kappa\text{B}$  P65), NOD-like receptor thermal protein domain associated protein 3, (NLRP3), Caspase-1, gasdermin D (GSDMD, IL-1 $\beta$  and IL-18 protein expressions, percentage of PI-positive cells, LDH activity, and IL-1 $\beta$  activity decreased significantly ( $P < .05$ ); the results in the Sh-FNDC5 group were opposite to those in the Ad-FNDC5 group. 3. Intervention with GW6471 (PPAR $\alpha$  antagonist) in the stably transfected THP-1-derived macrophages with FNDC5 overexpression abolished the protective effect of FNDC5 against ox-LDL-induced THP-1-derived macrophage pyroptosis.

**Conclusions** • Irisin/PPAR $\alpha$  inhibited THP-1-derived macrophage pyroptosis and inflammation and delayed AS by inhibiting the NF- $\kappa\text{B}$ /NLRP3 pathway (*Altern Ther Health Med.* 2023;29(3):32-42).

**Bo Zhou, MD; Guangjian Zhao, MM; Hui Li, MD; Quanwei Zhao, MM; Danan Liu, PhD;** Department of Cardiovascular Medicine, the Affiliated Hospital of Guzhou Medical University, Medical Research Institute, Guizhou Medical University, Guiyang, Guizhou, China.

Corresponding author: Danan Liu, PhD

E-mail: [liudanan2000@126.com](mailto:liudanan2000@126.com)

Atherosclerosis (AS) is a chronic inflammatory disease that affects large- and medium-sized arteries and presents with endothelial injury, macrophage infiltration, lipid accumulation, and proliferation of smooth muscle cells.<sup>1</sup> Inflammation is a critical factor for AS progression and is related to the entire process of AS development, which can finally result in plaque instability and rupture and adverse clinical events.<sup>2</sup>

The occurrence and development of AS indicate the infiltration of several inflammatory cells, including macrophages, and the release of inflammatory factors. Macrophages play vital roles in every stage of AS-plaque development. At the early stage of AS-plaque formation, macrophages alleviate local inflammatory responses and secondary necrocytosis through efferocytosis, thereby delaying plaque progression. However, as AS progresses, an increasing number of macrophages die within plaques, resulting in necrotizing lipid cores and finally formation of vulnerable plaques.<sup>3-5</sup>

Pyroptosis is a newly discovered, pro-inflammatory cell death that can trigger and amplify the occurrence and progression of AS,<sup>6</sup> and the entire process of AS development usually involves it.<sup>7</sup>

### Pyroptosis

Pyroptosis combines the morphological features of necrosis and apoptosis. First, the cell nuclei are concentrated but morphologically intact, with rupture of chromatin DNA and a positive result for “terminal deoxynucleotidyl transferase deoxyuridine triphosphate (dUTP) nick end labeling” (TUNEL) staining and Annexin V staining. Second, gasdermin D (GSDMD) can perforate the plasma membrane, resulting in the disappearance of intracellular and extracellular ionic concentration gradient. The entry of extracellular fluid into cells can cause osmotic swelling, cytolysis, and the release of the cells’ contents, which further induces inflammatory responses.<sup>7</sup>

Pyroptosis activates some members of the Caspase family. Researchers have proposed two molecular mechanisms for pyroptosis: the Caspase-1-dependent classical pathway and the Caspase-4/5/11-dependent non-classical pathway. Pyroptosis is related to infection, inflammation, and immune responses that activate inflammasomes. The first step in pyroptosis is inflammasome activation, cleaving and activating gasdermin D (GSDMD). The activated GSDMD translocates to the cell membrane, leading to perforation, cell swelling, extracellular content infiltration, and pyroptosis.<sup>8,9</sup>

Classical inflammasomes are members of the nucleotide-binding oligomerization domain-like receptor (NLR) family.<sup>7,9</sup> One classical pyroptosis pathway involves procaspase-1 being indirectly linked to pattern-recognition receptors, such as NLRP1 and NLRP3, through “apoptosis-associated speck-like protein” (ASC) to form an inflammasome, which further processes the nonactivated procaspase-1, causing rupture and activation of itself and formation of Caspase-1.

So far, the inflammasomes implicated in pyroptosis are NLRP1, NLRP3, NLRC4, and “absent in melanoma 2” (AIM2), an interferon-inducible protein. The latter further activates Caspase-1 or Caspase-4/5/11 and promotes the maturation and activation of GSDMD, precursor interleukin-1 beta (pro-IL-1 $\beta$ ), and pro-IL-18, producing the activated pro-inflammatory cytokines IL-1 $\beta$  and IL-18 and leading to cell swelling, cytolysis, and inflammatory responses. In addition, Caspase-1 cleaves the N-terminus of GSDMD, which binds to the cell membrane and causes perforation and pyroptosis.<sup>8</sup> The activated IL-1 $\beta$  and IL-18 further mediate the production and release of other inflammatory factors, amplifying the inflammatory response.<sup>24</sup>

In addition, low-density lipoprotein (LDL) can convert into oxidized LDL (ox-LDL), thereby promoting AS progression.<sup>25</sup> Dwevel et al showed that ox-LDL and cholesterol crystals could trigger the production of NLRP3 and Caspase-1 from macrophages, thereby activating IL-1 $\beta$  and IL-18.<sup>26</sup>

In addition, Lin et al reported that ox-LDL can promote the activation of Caspase-1 in human macrophages.<sup>27</sup> Those researchers suggested that ox-LDL-induced human macrophage lysis and generation of DNA fragments, IL-1 $\beta$ , and IL-18 may involve the NLRP3/Caspase-1 pathway. The evidence above suggests that ox-LDL induces macrophage pyroptosis and depends on the NLRP3-mediated molecular mechanism. Macrophage death in late AS plaques may involve pyroptosis.

### Pyroptosis and AS

Pyroptosis in vascular walls can occur at every stage of AS, especially the pyroptosis of endothelial cells and macrophages.<sup>10,11</sup> Shi et al observed that the NLRP3 inflammasomes were localized at the cytoplasm of foam cells and macrophages and at the carotid AS plaques in patients receiving carotid endarterectomy.<sup>12</sup> Those researchers found that NLRP3, ASC, caspase-1, IL-1 $\beta$ , and IL-18 were upregulated more in unstable plaques than in stable ones.

Those molecules were similarly upregulated in coronary artery plaques.<sup>13,14</sup> Ox-LDL and cholesterol crystals can induce macrophage NLRP3 and activate Caspase-1, leading to cytolysis, DNA fragmentation, and a rapid increase in IL-1 $\beta$  and IL-18 expression.<sup>6</sup> As analyzed above, macrophage pyroptosis can promote the formation of AS plaques at the later stage and cause plaque instability.

### Irisin and FNDC5

Irisin is a pro-myogenic factor discovered in 2012. Synthesized and secreted by skeletal muscles, irisin derives from the cleavage of the transmembrane protein, “fibronectin type III domain-containing protein 5” (FNDC5) and contains 112 amino acids.<sup>15</sup> Several studies found that irisin can significantly improve obesity, hyperglycemia, and hyperlipidemia and has an anti-inflammatory effect.<sup>16,17</sup>

Preliminary studies have also confirmed that irisin regulates the serum lipid profile, reduces the expressions of

inflammatory mediators and oxidative stress factors, inhibits the proliferation and migration of vascular smooth muscle cells (VSMCs), and prevents AS-plaque formation.<sup>18-20</sup> In another study, irisin treatment noticeably inhibited ox-LDL-induced, p38- mitogen-activated protein kinase (MAPK) phosphorylation and activation of “nuclear factor kappa-light chain enhancer of activated B cells p65” (NF- $\kappa$ B p65) in human umbilical endothelial cells (HUVECs).<sup>28</sup> Li et al found that irisin can alleviate the pyroptosis and inflammatory responses of RAW264.7 cells by inhibiting the NF- $\kappa$ B/NLRP3 signaling pathway.<sup>29</sup>

FNDC5 acts on uncoupling protein 1 (UCP1) by upregulating the “downstream peroxisome proliferator activated receptor alpha” (PPAR $\alpha$ ), which promotes lysis of lipids for heat production and energy dissipation, promoting white-to-brown, adipose-tissue conversion.<sup>15</sup> AS plaques express PPAR $\alpha$ , regulating lipid metabolism in plaque cells and inhibiting the inflammation signaling pathway.<sup>21</sup>

The activated PPAR $\alpha$  complex can alleviate inflammatory responses and atherosclerotic damage by inhibiting the transcriptional activity of the NF- $\kappa$ B p65/RelA gene, NF- $\kappa$ B activation, and the transcription and synthesis of inflammatory genes—IL-6 and tumor necrosis factor- $\alpha$  (TNF- $\alpha$ ) messenger RNA (mRNA). This action can mitigate inflammatory responses and atherosclerotic damage, which Wu et al found can further delay AS progression in ApoE $^{-/-}$  mice fed with high-fat diet.<sup>22</sup>

FNDC5 reduces NLRP3 upregulation and Caspase-1 and IL-1 $\beta$  production and release from ox-LDL-induced, VSMC-derived foam cells by inhibiting NF- $\kappa$ B activation.<sup>4</sup> In addition, FNDC5 can reduce lipid deposition and macrophage infiltration in the vascular walls of ApoE $^{-/-}$  mice via the phosphoinositide 3-kinase (PI3K) pathway, thereby significantly inhibiting AS.<sup>23</sup>

However, researchers are still uncertain about the anti-atherosclerotic mechanism of FNDC5. No studies have yet reported whether irisin can mediate PPAR $\alpha$ 's inhibition of macrophage pyroptosis.

The current study aimed to investigate the ability of FNDC5-mediated PPAR $\alpha$  to inhibit oxidized low-density lipoprotein (ox-LDL)-induced, THP-1-derived macrophage pyroptosis and to determine a potential molecular mechanism at the cellular level.

## METHODS

The research team performed a laboratory study. The study took place in the Department of Cardiovascular Medicine at the Affiliated Hospital of Guizhou Medical University at the Medical Research Institute at Guizhou Medical University in Guiyang, Guizhou, China.

## Materials and Reagents

The research team purchased: (1) THP-1 mononuclear cells from CHI Scientific (Qishi Biological Technology Co., LT, Jiangyin, China); (2) lentiviral vectors overexpressing FNDC5 and pLenti-EF1-EGFP-P2A-CMV-FNDC5-Puro-

3xFLAG-WPRE and lentiviral vectors silencing FNDC5 and pLenti-U6-shRNA (FNDC5)-CMV-EGFP-F2A-Puro-WPRE, from Obio Technology (Shanghai, China); (3) phorbol from Sigma (St. Louis, MO, USA), and ox-LDL from Guangzhou Yiyuan Biotechnology (Guangzhou, China); (4) Roswell Park Memorial Institute (RPMI) 1640 culture medium and fetal bovine serum (FBS) from GIBCO (Rockville, MD, USA); (5) a reverse transcription kit and an SYBR premix ex Taq<sup>TM</sup> kit from TaKaRa (Dalian, China); (6) an Oil Red O Staining Kit, human IL-1 $\beta$ , enzyme-linked immunosorbent assay (ELISA) kit, Hoechst 33342/propidium iodide (PI) Double-Staining Kit, lactate dehydrogenase (LDH) release assay kit, and cell counting kit 8 (CCK-8 Kit) from Beijing Solarbio Science & Technology (Beijing, China); (7) FNDC5, PPAR $\alpha$ , and p-NF- $\kappa$ B p65 antibodies from Beijing Biosynthesis Biotechnology (Beijing, China); (8) NLRP3, Caspase-1, ASC, GSDMD-N, IL-1 $\beta$ , IL18, (9) glyceraldehyde 3-phosphate dehydrogenase (GAPDH) antibodies from Affinity, (Cincinnati, OH, USA); (10) GW6471 from MedChemExpress (Monmouth Junction, NJ, USA); (11) puromycin from Gibco (Waltham, Massachusetts, USA); (12) TRIzol from Solarbio Science & Technology (Beijing, China); (13) radioimmunoprecipitation assay (RIPA) lysis buffer from Solarbio Science & Technology (Beijing, China); (14) phenylmethylsulfonyl fluoride (PMSF) from Solarbio Science & Technology (Beijing, China); (15) protein-loading buffer from Solarbio Science & Technology, (Beijing, China); (16) BSA-blocking solution from Solarbio Science & Technology (Beijing, China); (17) Tris-Buffered Saline Tween-20 (TBST) from Solarbio Science & Technology (Beijing, China); and (18) Sangon Biotech (Shanghai, China) performed the primer synthesis and sequencing.

## Procedures

**Cell culture.** The research team: (1) resuscitated and resuspended the frozen THP-1 cells in the RPMI 1640 medium with 10% FBS and added with 1% penicillin and streptomycin; (2) seeded the cells in a 25 cm<sup>2</sup> culture flask and cultured them at 37°C in a 5% CO<sub>2</sub> incubator; (3) harvested the cells once every 2-3 d for centrifugation and passage after growing to a number = 1 $\times$ 10<sup>8</sup>.

Obio Technology completed the construction and identification of the lentiviral vectors overexpressing and silencing FNDC5, the lentiviral packaging, and the lentiviral titer determination. The research team: (1) at 24 h before transcription, seeded the cells to a 24-well plate at a density of 1 $\times$ 10<sup>5</sup>/mL and cultured them at 37°C in a 5% CO<sub>2</sub> incubator; (2) 24 h later, added lentivirus and of polybrene (5  $\mu$ g/mL) to the cells at varying multiplicities of infection (MOIs)—1, 25, 50, and 100—to enhance the infection efficiency; (3) after 12 h, replaced the culture medium; (4) 72 h later observed the expression of green fluorescent protein under a fluorescence microscope (Olympus, Tokyo, Japan); (5) screened the cells with 1  $\mu$ g/mL of puromycin because the recombinant lentiviral vector contained the

puromycin-resistance gene; (6) replaced the culture medium with the puromycin-containing medium and 1-2 d after cell transfection centrifuged or passaged the cells; and (7) used the stably transfected cells for the subsequent testing.

**Effects of ox-LDL concentrations on THP-1-derived macrophage pyroptosis.** The research team: (1) before each experiment, incubated the THP-1 cells with 160 nmol/L phorbol for 24 h to induce them into macrophages; (2) added different concentrations of ox-LDL—0, 25, 50, and 100  $\mu\text{g}/\text{ml}$ —to incubate the cells for 48 h, thereby establishing the pyroptosis model in THP-1-derived macrophages; (3) co-incubated the THP-1-derived macrophages with 10  $\mu\text{M}$  of GW6471 and then further with 100  $\mu\text{g}/\text{ml}$  of ox-LDL for 48 h for subsequent experiments.

**Groups.** The research team divided the THP-1-derived macrophages into seven groups: NC group (no ox-LDL intervention), ox-LDL group, PBS group, Mock1 group, Ad-FNDC5 group, Mock2 group, and Sh-FNDC5 group.

**Cell-viability determination.** The research team: (1) performed the CCK-8 assay to determine cell viability; (2) cultured the cells at different concentrations of GW6571 in a 96-well plate for 24 h; (3) into each well, added 10  $\mu\text{L}$  of CCK-8 solution to further culture the cells for 3 h, with the absorbance being measured at a wavelength of 450 nm.

**Quantitative real-time polymerase chain reaction (qRT-PCR).** The research team extracted total RNA from the cells using the TRIzol reagent and reversely transcribed it into the complementary DNA (cDNA). The team then carried out qRT-PCR using the SYBR premix ex Taq<sup>TM</sup> kit under the following conditions: (1) predenaturation at 95°C for 30 s, (2) denaturation at 95°C for 5 s, and (3) annealing at 60°C for 30 s, for a total of 40 cycles.

The research team excluded non-specific amplification by plotting the melting and amplification curves and used  $\beta$ -actin as the internal reference gene. The team calculated the relative expression of the target gene using the  $2^{-\Delta\Delta\text{Ct}}$  method:  $\Delta\text{Ct} = \text{average cycle threshold (CT) value of the target gene in the experimental group} - \text{average CT value of the target gene in the control group} - \text{average CT value of the internal reference gene}$ .

The upstream primer sequence of the internal reference gene, glyceraldehyde-3-phosphate dehydrogenase-human (GAPDH), was 5'-CTGGGCTACACTGAGCACC-3', and the downstream primer sequence was 5'-AAGTGGTCGTTGAGGGCAATG-3'. For the target gene FNDC5, the upstream primer sequence was 5'-GAAAGAGATGGGAGGAACCAACAG-3', and the downstream primer sequence was 5'-GATGTCATACTGGCGGCAGAAGAG-3'.

**Western Blot.** The research team: (1) harvested cells from the 24-well plate for the NC, Ox-LDL, PBS, Mock1, Ad-FNDC5, Mock2, and Sh-FNDC5 groups; (2) into each well, added 25  $\mu\text{L}$  of RIPA lysis buffer with 1 mg/mL of PMSF, and put it on ice for 30 min; (3) centrifuged the cells at 12 000 g for 20 min; and (4) collected 5  $\mu\text{L}$  of the supernatant for quantification of bicinchoninic acid (BCA) proteins;

(5) added the remaining portion of the supernatant with 5 $\times$  protein-loading buffer, boiled it for 10 min, and loaded an equal volume of protein; (6) after performing sodium dodecyl-sulfate polyacrylamide gel electrophoresis (SDS-PAGE (Solarbio Life Sciences, Beijing China) , transferred the proteins to polyvinylidene fluoride (PVDF) membranes at a constant current; and (7) then soaked the membranes in 5% BSA-blocking solution and put them on a shaker at room temperature for 1 h; (8) washed the PVDF membranes with TBST three times.

After blocking the membranes, the research team added them to the following antibodies: rabbit anti-human FNDC5 antibody (1:1000), PPAR $\alpha$  antibody (1:1000), p-NF- $\kappa\text{B}$  p65 antibody (1:1000), NLRP3 antibody (1:1000), Caspase-1 antibody (1:1000), ASC antibody (1:1000), GSDMD-N antibody (1:1000), IL-1 $\beta$  antibody (1:1000), IL-18 (1:1000) antibody, and GAPDH primary antibody (1:5000). The team then: (1) incubated the membranes at 4°C overnight and washed them with TBST three times for 15 min each; (2) later incubated the membranes with goat anti-rabbit IgG antibody (1:5000) at room temperature for 1 h; (3) then washed the membranes again with TBST three times for 15 min each; (4) determined the protein expression using electrochemiluminescence (ECL), with GAPDH as the internal reference; (5) used the grayscale ratio between the target gene and the internal reference gene to represent the relative expression of the target protein; and (6) analyzed the grayscale values of the protein bands using the Gel-Pro analyzer4 software (Media Cybernetics, Rockville, MD, USA)

**Hoechst 33342/PI double staining.** The research team: (1) evaluated the cell-membrane perforation during pyroptosis using Hoechst 33342/PI double staining; (2) transferred approximately 105 cells to a 1.5 ml centrifuge tube and centrifuged them instantaneously at 500 g for about 15 s; (3) discarded the supernatant and added 5  $\mu\text{L}$  of the Hoechst dye; (4) then added 5  $\mu\text{L}$  of PI and mixed the solution properly; (5) incubated the cells at 4°C for 20 min, followed by centrifugation at 500 g for 30 s; (6) washed the cells with PBS three times for 3 min each; (7) captured images under an inverted fluorescence microscope (Canon, Tokyo, Japan); and (8) estimated the percentage of PI-positive cells using Image J (National Institutes of Health, Baltimore, Maryland, USA).

**LDH release assay.** The research team: (1) determined cytotoxicity to assess the cell membranes' integrity; (2) after the corresponding treatments, added ox-LDL 100 $\mu\text{g}/\text{ml}$  for incubation for 24h, collected the supernatant; and (3) determined the LDH level using the LDH assay kit according to the instructions.

**Enzyme-linked immunosorbent assay (ELISA).** The research team determined the IL-1 $\beta$  protein expression using the ELISA kit according to the manufacturer's instructions. The team collected the cell-culture supernatant after the corresponding treatment; added ox-LDL 100 $\mu\text{g}/\text{ml}$  for incubation for 24h, and (2) determined the amount of mature IL-1 $\beta$  released.

## Outcome Measures

### Lentiviral vectors overexpressing or silencing FNDC5.

The research team determined the mRNA and protein expressions of FNDC5 using RT-PCR and A Western Blot, respectively, in stably transfected THP-1 cells with FNDC5 overexpression and silencing.

After adding the polybrene to the cells at the varying MOIs—1, 25, 50, and 100—in each group, the research team assessed the transfection efficiency. If the overexpression of the lentiviral vector—pLenti-EF1-EGFP-P2A-Puro-CMV-FNDC5-3xFLAG-WPRE—contained EGFP, the successfully transfected THP-1 cells would emit green fluorescence under the inverted fluorescence microscope. Otherwise, no green fluorescence occur. Thus, the research team could preliminarily assess transfection efficiency: transfection efficiency = number of cells emitting green fluorescence/total number of cells×100%.

For the lentiviral transfection, therefore, the team used the cells with an MOI=100 and screened them with 1 µg/mL of puromycin. Thus, the research team obtained the THP-1 cells with a stable FNDC5 expression and silencing. The team then determined the mRNA and protein expression of FNDC5 in the stably transfected THP-1 cells that had FNDC5 overexpression and silencing, with RT-PCR and Western Blot, respectively.

**Ox-LDL-induced THP-1-derived macrophage pyroptosis.** The research team examined the THP-1-derived macrophage pyroptosis induced by different concentrations of ox-LDL, using the Hoechst 33342/PI double staining and determination of LDH and IL-1β activity. The research team treated the THP-1-derived macrophages with different concentrations of ox-LDL—0, 25, 50, and 100 µg/ml—for 24 h. The cells were stained red with Hoechst 33342 and blue with PI.

**Effects of FNDC5 overexpression and silencing.** The research team examined the effects of FNDC5 overexpression and silencing on THP-1-derived macrophage pyroptosis. The NC group consisted of THP-1-derived macrophages not treated with ox-LDL. The cells in the ox-LDL, PBS, Mock1, Ad-FNDC5, Mock2, and Sh-FNDC5 groups were incubated with 100 µg/ml of ox-LDL for 24 h.

**Macrophage pyroptosis, LDH activity, and IL-1β activity.** The research team examined the THP-1-derived macrophage pyroptosis after GW6471 intervention. The team used Hoechst 33342/PI double staining. The cells stained with Hoechst 33342 were blue, and those stained with PI were red. The research team examined the levels of LDH activity and of the IL-1β activity in the cell-culture supernatant in the different groups, using ELISA.

### FNDC5 overexpression after the GW6471 intervention.

The next step was to verify that FNDC5 alleviated THP-1-derived macrophage pyroptosis by upregulating PPARα expression. For this purpose, the research team used GW6471, a PPARα-specific inhibitor. The research team examined cell viability using a cell counting kit 8 (CCK-8) after treatment of the THP-1-derived macrophages with

different concentrations of GW6471—0.1, 1, 10, and 100 µg/ml—for 24 h. The team measured PPARα protein expressions after treatment with the four concentrations for one hour and co-incubation with 100 µg/ml of ox-LDL for 24 h, using the Western Blot.

## Statistical Analysis

The research team conducted the statistical analyses using the Prism7.0 software (La Jolla, CA, USA). The team: (1) expressed the experimental data as means ± standard deviations (SDs), (2) conducted multiple comparisons using the one-way analysis of variance, (3) analyzed measurements not obeying homogeneity of variance using Kruskal-Wallis H test. A  $P < .05$  was considered to be statistically significant.

## RESULTS

### Lentiviral Vectors Overexpressing or Silencing FNDC5

For the transfection of the THP-1 cells (Figure 1): (1) an MOI=1 indicated that the research team had successfully transfected only a small amount ( $9.15 \pm 1.81$ ); (2) an MOI=25 indicated that the transfection occurred with a higher efficiency than with an MOI=1, but the efficiency was still unsatisfactory ( $22.43 \pm 1.39$ ); (3) an MOI=75 further enhanced the transfection efficiency in THP-1 cells, but it was still not ideal, with a transfection efficiency of  $44.14 \pm 5.41\%$ ; (4) an MOI=100 indicated that most THP-1 cells emitted green fluorescence, and the transfection efficiency was  $75.10 \pm 3.47\%$ . An MOI=100 transfected a significantly greater number of cells compared with an MOI=75, with  $P < .0001$  (Figures 1A and B). Figure 1C shows the Western Blot's results with the FNDC5 protein expression of THP-1 cells, as transfected with lentiviral vectors overexpressing and silencing FNDC5 with an MOI=100.

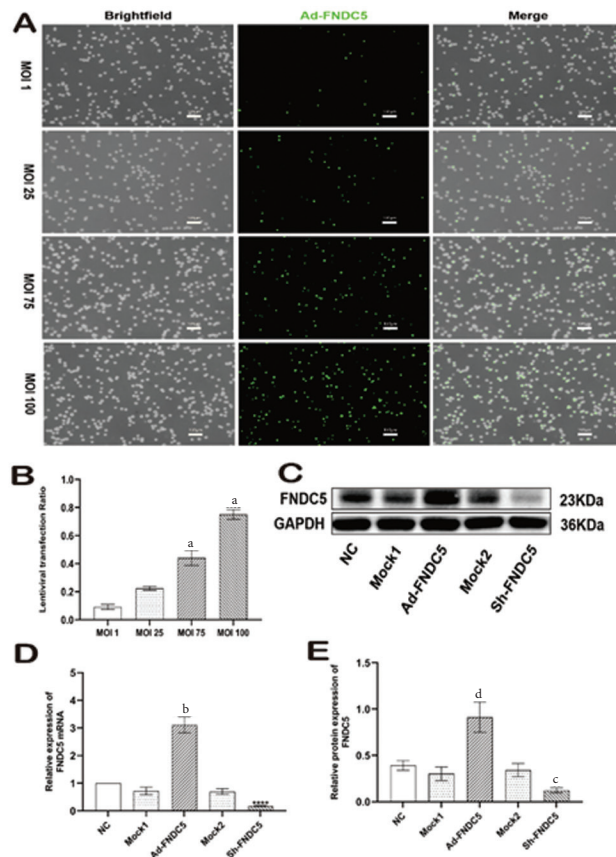
Figures 1D and 1E show the verification of the transfection efficiency of FNDC5. No significant differences existed in the mRNA and protein expressions of FNDC5 between the NC group and the Mock1 and Mock2 groups ( $P > .05$ ). Compared with the Mock1 group, the Ad-FNDC5 group's mRNA and protein expression of FNDC5 were significantly greater ( $P < .0001$ ). Compared with the Mock2 group, the Sh-FNDC5 group's mRNA and protein expressions of FNDC5 were significantly greater, with  $P < .0001$  and  $P < .01$ , respectively.

### Ox-LDL-induced THP-1-derived Macrophage Pyroptosis

Figure 2A shows the Hoechst 33342/PI staining for the different concentrations of ox-LDL. Hoechst 33342 stained red, and PI stained blue. A small area of red staining,  $2.22 \pm 0.57$  occurred in the 0 µg/ml group. The red staining was a little more intense,  $13.26 \pm 1.72$ , in the 25 µg/ml group, and the staining was further intensified,  $30.18 \pm 2.45$ , in the 50 µg/ml group. A large area of red staining,  $43.16 \pm 2.04$ , occurred in the 100 µg/ml group.

Figure 2A shows the PI-positive cells; Figure 2B shows the statistical results of the proportion of PI-positive cells, Figure 2C shows the LDH activity; and Figure 2D shows the

**Figure 1.** The mRNA and Protein Expressions of FNDC5 using RT-PCR and Western Blot, respectively, in Stably Transfected THP-1 Cells With FNDC5 Overexpression and Silencing. Figure 1A shows the lentiviral vector overexpressing FNDC5 that the research team added at varying MOIs—1, 25, 50, 100. Figure 1B shows the estimated transfection efficiency in THP-1 cells, as transfected at the four MOIs. Figure 1C shows the Western Blot’s results with the FNDC5 protein expression of THP-1 cells, as transfected with lentiviral vectors overexpressing and silencing FNDC5 with an MOI=100. Figure 1D and 1E show the verification of the transfection efficiency of FNDC5, using RT-PCR and Western Blot, respectively.



<sup>a</sup> $P < .0001$ , indicating in Figure 1B that an MOI=75 and MOI=100 transfected a significantly greater number of cells compared with MOI=1

<sup>b</sup> $P < .0001$ , indicating in Figure 1D that the Ad-FNDC5 group’s mRNA expression of FNDC5 was significantly greater than that of the Mock 1 group and that the Sh-FNDC5 group’s mRNA expression of FNDC5 was significantly lower than that of the Mock 2 group.

<sup>c</sup> $P < .01$ , indicating in Figure 1E that the Sh-FNDC5 group’s protein expression of FNDC5 was significantly lower than that of the Mock 2 group.

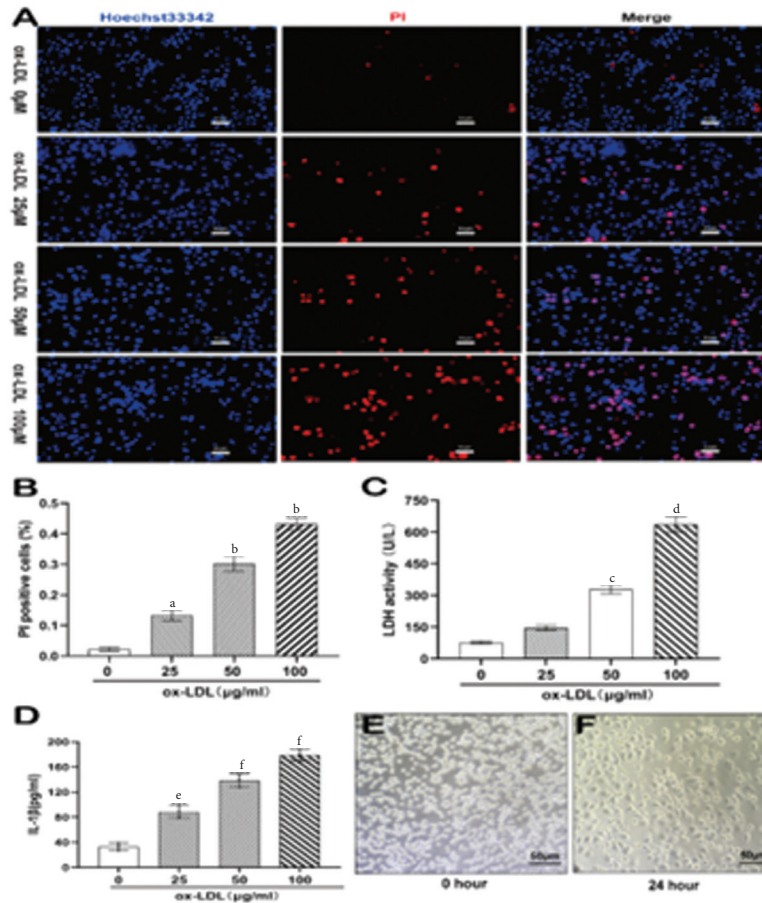
<sup>d</sup> $P < .0001$ , indicating in Figure 1E that the Ad-FNDC5 group’s protein expression of FNDC5 was significantly greater than that of the Mock 1 group.

**Abbreviations:** CMV, cytomegalovirus; EF1, eukaryotic translation elongation factor 1; EGFP, enhanced green fluorescent protein; FNDC5, fibronectin type III domain-containing protein 5; MOI, multiplicity of infection; mRNA, messenger RNA; P2A, porcine teschovirus-1 2A; RT-PCR, reverse transcription polymerase chain reaction; WPRE, woodchuck hepatitis virus post-transcriptional regulatory element.

detection using ELISA of the IL-1 $\beta$  activity in the cell-culture supernatant for the different concentrations of ox-LDL. The number of PI-positive cells were significantly higher for the groups using 25, 50, and 100  $\mu\text{g}/\text{ml}$  of ox-LDL than for 0  $\mu\text{g}/\text{ml}$  ox-LDL group, with  $P < .001$ ,  $P < .0001$ , and  $P < .0001$ , respectively. Figure 2C shows that the levels of LDH were

significantly higher for the 50  $\mu\text{g}/\text{ml}$  and 100  $\mu\text{g}/\text{ml}$  ox-LDL groups than for the 0  $\mu\text{g}/\text{ml}$  group, with  $P < .001$  and  $P < .0001$ , respectively. However, the indicators were significantly greater in the 100  $\mu\text{g}/\text{ml}$  group. Therefore, the research team chose the THP-1-derived macrophages that 100  $\mu\text{g}/\text{ml}$  ox-LDL induced to build the pyroptosis model.

**Figure 2.** THP-1-derived Macrophage Pyroptosis Induced by Different Concentrations of Ox-LDL, using the Hoechst 33342/PI double staining and determination of LDH and IL-1 $\beta$  activity. Figure 2A shows the Hoechst 33342/PI double staining after treatment of the THP-1-derived macrophages with different concentrations of ox-LDL—0, 25, 50, and 100  $\mu\text{g/ml}$ —for 24 h. The cells were stained red with Hoechst 33342 and blue with PI. Figure 2B shows the PI-positive cells, and Figure 2C shows the LDH activity in the different groups. Figure 2D shows the detection using ELISA of the IL-1 $\beta$  activity in the cell-culture supernatant in the different groups. Figure 2E shows that the THP-1 cells before differentiation induction were round suspension cells, with a smooth surface and no pseudopodia. Figure 2F shows that the cells, after treatment with 160 nmol/ml of PMA for 72 h, extended pseudopodia and showed an irregular shape and adherent growth. The cells grew in clusters and featured a typical morphology of macrophages.



<sup>a</sup> $P < .001$ , indicating in Figure 2B that the number of PI-positive cells were significantly higher for 25  $\mu\text{g/ml}$  of ox-LDL than for 0  $\mu\text{g/ml}$

<sup>b</sup> $P < .0001$ , indicating in Figure 2B that the number of PI-positive cells were significantly higher for 50  $\mu\text{g/ml}$  and 100  $\mu\text{g/ml}$  of ox-LDL than for 0  $\mu\text{g/ml}$

<sup>c</sup> $P < .001$ , indicating in Figure 2C that the levels of LDH were significantly higher for 50  $\mu\text{g/ml}$  of ox-LDL than for 0  $\mu\text{g/ml}$

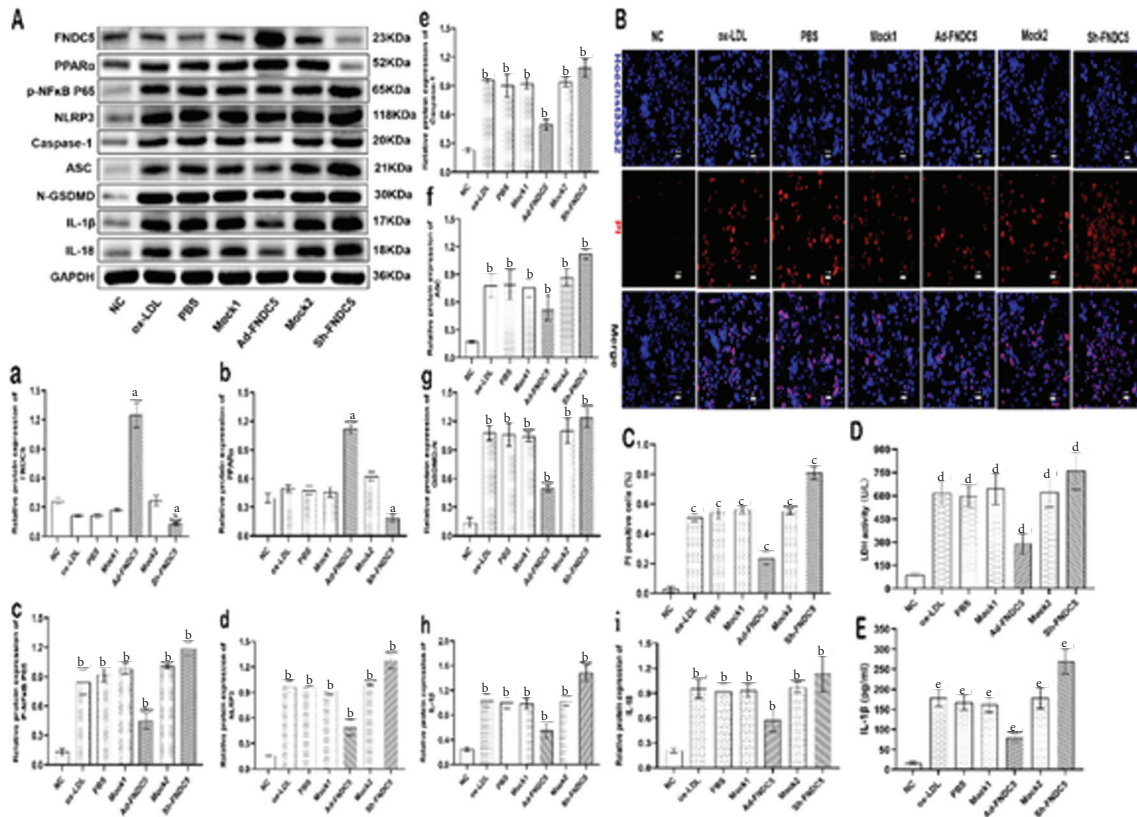
<sup>d</sup> $P < .0001$ , indicating in Figure 2C that levels of LDH were significantly higher for 100  $\mu\text{g/ml}$  of ox-LDL than for 0  $\mu\text{g/ml}$

<sup>e</sup> $P < .001$ , indicating in Figure 2D that the levels of IL-1 $\beta$  activity were significantly higher for 25  $\mu\text{g/ml}$  of ox-LDL than for 0  $\mu\text{g/ml}$

<sup>f</sup> $P < .0001$ , indicating in Figure 2D that the levels of IL-1 $\beta$  activity were significantly higher for 50  $\mu\text{g/ml}$  and 100  $\mu\text{g/ml}$  of ox-LDL than for 0  $\mu\text{g/ml}$

**Abbreviations:** IL-1 $\beta$ , interleukin-1 beta; LDH, lactate dehydrogenase; ox-LDL, oxidized low-density lipoprotein; PI, propidium iodide; PMA, phorbol 12-myristate-13-acetate.

**Figure 3.** Effects of FNDC5 Overexpression and Silencing on THP-1-derived Macrophage Pyroptosis. Figure 3A (a-i) showed the Western Blot images and the statistical results of protein expression using Western Blot, in the different groups—FNDC5, PPARα, p-NF-κB p65, NLRP3, Caspase-1, ASC, GSDMD, IL-1β, and IL-18—in the THP-1-derived macrophages. Figure 3B shows the Hoechst 33342/PI double staining; the cells stained with Hoechst 33342 were blue, and those stained with PI were Red. Figure 3C shows the PI-positive cells in the different groups; Figure 3D shows the LDH activity in the different groups; and Figure 3E shows the detection of the IL-1β activity in the cell-culture supernatant in the different groups, using ELISA.



<sup>a</sup> $P < .0001$ , indicating in Figure 3Aa and 3Ab that the Ad-FNDC5 group's FNDC5 and PPARα protein expression were significantly higher than those of the Mock 1 group and that the Sh-FNDC5 group's FNDC5 and PPARα protein expression were significantly lower than those of the Mock 2 group.

<sup>b</sup> $P < .0001$ , indicating in Figure 3Ac-3Ai that the Ad-FNDC5 group's protein expression of NF-κB p65, NLRP3, Caspase-1, ASC, GSDMD-N, IL-1β, and IL-18 were significantly lower than those of the Mock 1 group and that the Sh-FNDC5 group's protein expression of NF-κB p65, NLRP3, Caspase-1, ASC, GSDMD, IL-1β, and IL-18 were significantly higher than those of the Mock 2 group.

<sup>c</sup> $P < .0001$ , indicating in Figure 3C that the number of PI-positive cells were significantly higher for the ox-LDL, PBS, Mock1, and Mock2 groups than that for the NC group; that the Ad-FNDC5 group's number of PI-positive cells was significantly lower than that of the Mock1 group; and that the Sh-FNDC5 group's number of PI-positive cells was significantly higher than that of the Mock2 group

<sup>d</sup> $P < 0.0001$ , indicating in Figure 3D that levels of LDH were significantly higher for the ox-LDL, PBS, Mock1, and Mock2 groups than for the NC group; that the Ad-FNDC5 group's levels of LDH were significantly lower than those of the Mock1 group; and that the Sh-FNDC5 group's levels of LDH were significantly higher than those of the Mock2 group

<sup>e</sup> $P < .0001$ , indicating in Figure 3E that the levels of IL-1β activity were significantly higher for the ox-LDL, PBS, Mock1, and Mock2 groups than for the NC group; that the Ad-FNDC5 group's levels of IL-1β activity were significantly lower than those of the Mock1 group; and that the Sh-FNDC5 group's levels of IL-1β activity were significantly higher than those of the Mock2 group

**Abbreviations:** ASC, apoptosis-associated speck-like protein ; ELISA, enzyme-linked immunosorbent assay; FNDC5, fibronectin type III domain-containing protein 5; GSDMD, gasdermin D; IL-1β, interleukin-1 beta; LDH, lactate dehydrogenase; NC, group with no ox-LDL intervention; NLRP3, NLR family pyrin domain containing 3; ox-LDL, oxidized low-density lipoprotein; p-NF-κB p65, nuclear factor kappa-light chain enhancer of activated B cells p65; PPARα, peroxisome proliferator activated receptor alpha; PBS, phosphate buffered saline; PI, propidium iodide.

The levels of IL-1 $\beta$  activity were significantly higher for the groups using 25, 50, and 100  $\mu$ g/ml of ox-LDL than for the 0  $\mu$ g/ml of ox-LDL group with  $P < .001$ ,  $P < .0001$ , and  $P < .0001$ , respectively.

Figure 2E shows that the THP-1 cells before differentiation induction were round suspension cells, with a smooth surface and no pseudopodia. Figure 2F shows that the cells, after treatment with 160 nmol/ml of PMA for 72 h, extended pseudopodia and showed an irregular shape and adherent growth. The cells grew in clusters and featured a typical morphology of macrophages.

### Effects of FNDC5 Overexpression and Silencing

Figure 3A, including Aa-Ai, shows the protein expression, using Western Blot, in the different groups—FNDC5, PPARa, p-NF- $\kappa$ B p65, NLRP3, Caspase-1, ASC, GSDMD, IL-1 $\beta$ , and IL-18—in the THP-1-derived macrophages. (Figure 3A shows Western Blot, Figure 3a-i shows the statistical results of protein expressions of FNDC5, PPARa, p-NF- $\kappa$ B p65, NLRP3, Caspase-1, ASC, GSDMD, IL-1 $\beta$ , and IL-18).

Figures 3Aa and 3Ab show that no significant differences existed in the number of protein expression of FNDC5 and PPARa between the NC group and the ox-LDL, PBS, Mock1, and Mock2 groups ( $P > .05$ ). Compared with the Mock1 group, the Ad-FNDC5 group's FNDC5 protein expression, at  $124.70 \pm 12.68$ , and its PPARa protein expression, at  $112.21 \pm 4.91\%$ , were significantly higher (both  $P < .0001$ ). Compared with the Mock2 group, the Sh-FNDC5 group's FNDC5 protein expression, at  $13.06 \pm 1.58$ , and its PPARa protein expression, at  $18.49 \pm 3.78$ , were significantly lower (both  $P < .0001$ ).

Figures 3Ac to 3Ai show that no significant differences existed in the number of protein expression of NF- $\kappa$ B p65, NLRP3, Caspase-1, ASC, GSDMD, IL-1 $\beta$ , and IL-18 between the NC group and the ox-LDL, PBS, Mock1, and Mock2 groups ( $P < .05$ ). Compared with the Mock1 group, the Ad-FNDC5 group's protein expression of NF- $\kappa$ B p65, NLRP3, Caspase-1, ASC, GSDMD, IL-1 $\beta$ , and IL-18 were significantly lower ( $P < .05$ ). Compared with the Mock2 group, the Sh-FNDC5 group's protein expression of NF- $\kappa$ B p65, NLRP3, Caspase-1, ASC, GSDMD, IL-1 $\beta$ , and IL-18 in the were significantly higher ( $P < .05$ ).

Figure 3B shows the Hoechst 33342/PI double staining; the cells stained with Hoechst 33342 were Blue, and those stained with PI were Red.

Figure 3B shows the Hoechst 33342/PI double staining, and Figure 3C shows the detection of Hoechst 33342/PI double staining in the different groups.

### Macrophage Pyroptosis

Figure 3C shows the PI-positive cells in the different groups; Figure 3D shows the LDH activity in the different groups; and Figure 3E shows the detection of the IL-1 $\beta$  activity in the cell-culture supernatant in the different groups, using ELISA. Compared with the NC group, at  $2.85 \pm 1.09$ , the number of PI-positive cells was significantly

higher in the ox-LDL group, at  $53.09 \pm 2.72$ ; the PBS group, at  $53.46 \pm 4.60$ ; the Mock1 group, at  $53.39 \pm 2.77$ ; and the Mock2 group, at  $55.15 \pm 1.74$  (all  $P < .0001$ ). Compared with the Mock1 group, the Ad-FNDC5 group's number of PI-positive cells, at  $23.77 \pm 4.17$ , was significantly lower ( $P < .0001$ ). The Sh-FNDC5 group's number of PI-positive cells, at  $80.92 \pm 4.49$ , was significantly higher than that of the Mock2 group ( $P < .0001$ ).

### LDH Activity

Figure 3D shows the LDH activity in the different groups. Compared with the NC group, at  $89.17 \pm 12.34$  U/L, the LDH activity was significantly higher in the ox-LDL group, at  $618.91 \pm 78.46$  U/L; the PBS group, at  $597.36 \pm 69.17$  U/L; the Mock1 group, at  $647.13 \pm 101.56$  U/L; and the Mock2 group, at  $623.78 \pm 99.89$  U/L (all  $P < .0001$ ). Compared with the Mock1 group, the Ad-FNDC5 group's LDH activity, at  $23.77 \pm 4.17$  U/L, was significantly lower ( $P < .0001$ ). The Sh-FNDC5 group's LDH activity, at  $80.92 \pm 4.49$ , was significantly higher than that in the Mock2 group ( $P < .0001$ ).

### IL-1 $\beta$ Activity

Figure 3E shows the IL-1 $\beta$  activity in the cell-culture supernatant in the different groups. Compared with the NC group, at  $16.24 \pm 3.78$  U/L, the IL-1 $\beta$  activity was significantly higher in the ox-LDL group, at  $178.17 \pm 21.89$  U/L; the PBS group, at  $167.19 \pm 18.96$  U/L; the Mock1 group, at  $162.64 \pm 19.63$  U/L; and the Mock2 group, at  $178.96 \pm 26.71$  U/L ( $P < .0001$ ). Compared with the Mock1 group, the Ad-FNDC5 group's IL-1 $\beta$  activity, at  $79.16 \pm 9.74$  U/L, was significantly lower ( $P < .001$ ). Compared with the Mock2 group, the Sh-FNDC5 group's IL-1 $\beta$  activity, at  $269.74 \pm 31.84$  U/L, was significantly lower.

### FNDC5 Overexpression After the GW6471 Intervention

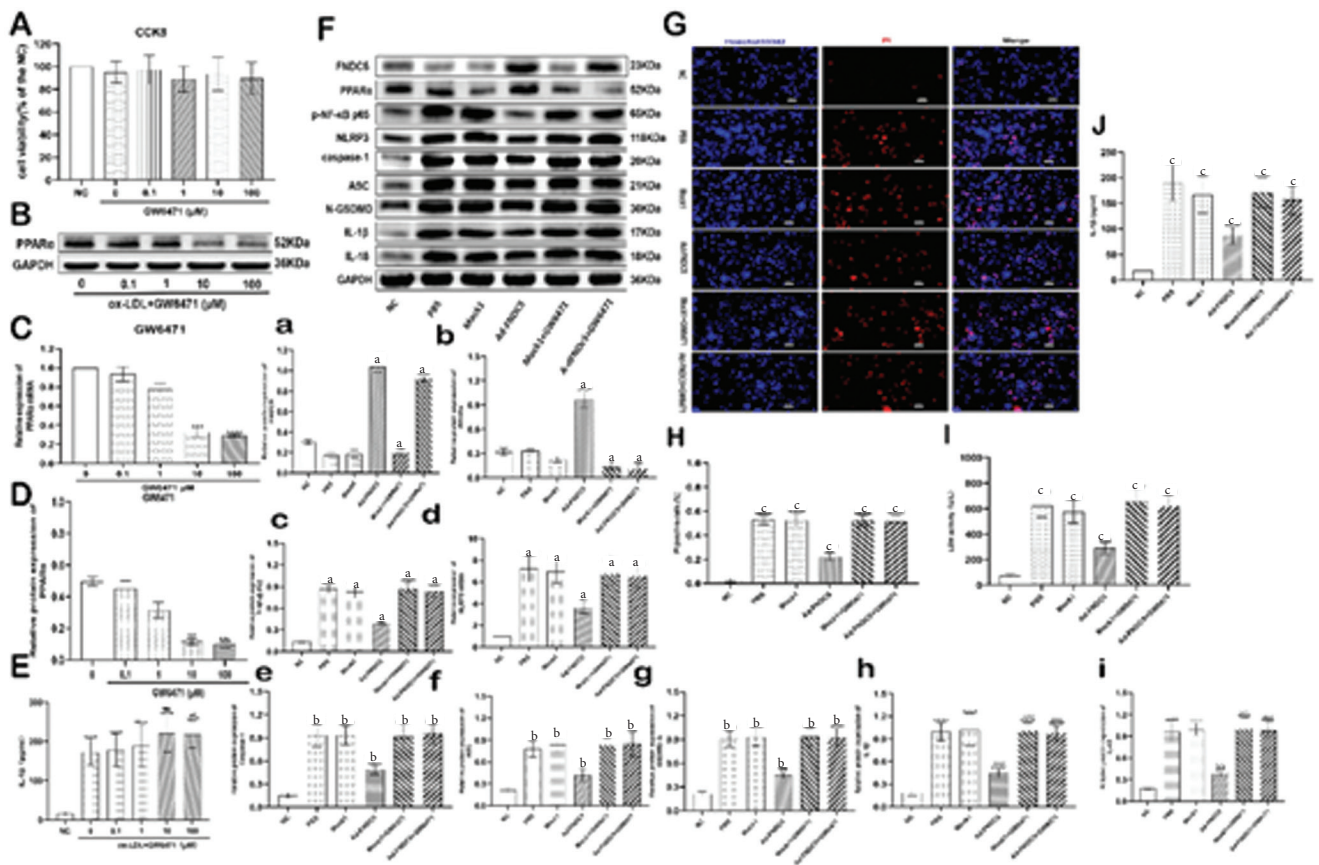
Figure 4 shows the THP-1-derived macrophage pyroptosis after an intervention using different concentrations of GW6471—0.1, 1, 10, and 100  $\mu$ g/ml. No significant differences existed in the FNDC5 protein expression. Figure 4A shows the cell viability. The GW6471 intervention dramatically inhibited the protein expression of PPARa (Figure 4B).

Figures 4B, 4C and 4D show the mRNA and protein expressions of PPARa. Compared with the GW6471 0  $\mu$ M group, no significant differences existed in the mRNA and protein expressions of PPARa in the 0.1  $\mu$ M and 1  $\mu$ M groups ( $P > .05$ ). However, the mRNA and protein expressions of PPARa in the GW6471 10  $\mu$ M and 100  $\mu$ M groups were significantly lower than that of the GW6471 0  $\mu$ M group ( $P < .01$ ).

Figure 4E shows the IL-1 $\beta$  activity detected by ELISA.

Figure 4F shows the protein expressions of FNDC5, PPARa, p-NF- $\kappa$ B p65, and pyroptosis-related proteins after the GW6471 10  $\mu$ M treatment. Compared with the Ad-FNDC5 group, the Ad-FNDC5+GW6471 group's protein expression of p-NF- $\kappa$ B p65, NLRP3, Caspase-1, ASC,

**Figure 4.** THP-1-derived Macrophage Pyroptosis Detected After GW6471 Intervention. The intervention used different concentrations of GW6471—0.1, 1, 10, and 100 µg/ml. Figure 4A shows the cell viability using CCK-8 after treatment of the THP-1-derived macrophages with GW6471 for 24 h. No significant differences existed in the cell counts across the groups ( $P > .05$ ), and the Kruskal-Wallis H test was employed. Figure 4B shows the PPARα protein expressions detected by Western Blot after the THP-1-derived macrophages were treated with GW6471 for one h and co-incubated with ox-LDL 100 µg/ml for 24 h. Figures 4C and 4D show the mRNA and protein expressions of PPARα, as detected by RT-PCR and Western Blot, respectively. Compared with the GW6471 0 µM group, no significant differences existed in the mRNA and protein expressions of PPARα in the 0.1 and 1 µM groups ( $P > .05$ ). However, the mRNA and protein expressions of PPARα in the GW6471 10 and 100 µM groups decreased dramatically ( $P < .01$ ). Figure 4E shows the IL-1β activity detected by ELISA. The NC group consisted of THP-1-derived macrophages not treated with ox-LDL. Figure 4F shows the protein expressions of FNDC5, PPARα, p-NF-κB p65, and pyroptosis-related proteins after the GW6471 10µM treatment, as detected by Western Blot. Figure 4G shows the Hoechst 33342/PI double staining; the cells stained with Hoechst 33342 were blue, and those stained with PI were red. Figure 4H shows the detection results of Hoechst 33342/PI double staining in the different groups. Figure 4I shows the detection results of LDH activity in the different groups. Figure 4J shows the detection results of IL-1β activity in the cell-culture supernatant as detected by ELISA in the different groups.



<sup>a</sup> $P < .01$ , indicating in Figures 4Fa and 4Fb and Figures 4Fc and 4Fd that the mRNA and protein expressions of PPARα in the GW6471 10 µM and 100 µM groups were significantly lower than those in the GW6471 0 100 µM group  
<sup>b</sup> $P < .01$ , indicating in Figure 4Fe and 4Ff that the Ad-FNDC5+GW6471 group's levels of protein expression of p-NF-κB p65, NLRP3, Caspase-1, ASC, GSDMD, IL-1β, and IL-18 were significantly higher, than for the Ad-FNDC5 group  
<sup>c</sup> $P < .01$ , indicating in Figures 4H-4J that the Ad-FNDC5+GW6471 group's number of PI-positive cells, LDH activity, and IL-1β activity in the cell-culture supernatant were significantly higher than those of the Ad-FNDC5 group

**Abbreviations:** CCK-8, cell counting kit 8; ELISA, enzyme-linked immunosorbent assay; FNDC5, fibronectin type III domain-containing protein 5; IL-1β, interleukin-1 beta; LDH, lactate dehydrogenase; mRNA, messenger RNA; PI, propidium iodide; PPARα, peroxisome proliferator activated receptor alpha.

GSDMD, IL-1 $\beta$ , and IL-18 were significantly higher, with  $P < .01$  (Figure 4F). Compared with the Mock1+GW6471 group, the Ad-FNDC5+GW6471 group's protein expressions of the above factors weren't significantly different ( $P > .05$ ).

Figures 4G shows the Hoechst 33342/PI double staining; the cells stained with Hoechst 33342 were blue, and those stained with PI were red. Figure 4H shows that the number of PI-positive cells weren't significantly different between the Ad-FNDC5+GW6471 group and the Mock1+GW6471 group ( $P > .05$ ). Figure 4I shows the LDH activity wasn't significantly different between the Ad-FNDC5+GW6471 group and the Mock1+GW6471 group ( $P > .05$ ). Figure 4J shows that the IL-1 $\beta$  activity in the cell-culture supernatant wasn't significantly different between the Ad-FNDC5 + GW6471 group and the Mock1+GW6471 group ( $P > .05$ ).

However, the Ad-FNDC5+GW6471 group's number of PI-positive cells, LDH activity and IL-1 $\beta$  activity in the cell-culture supernatant were significantly higher than those of the Ad-FNDC5 group ( $P < .01$ ). The above results indicate that FNDC5 alleviated THP-1-derived macrophage pyroptosis by upregulating PPAR $\alpha$ .

## DISCUSSION

In the current study, ox-LDL induced THP-1-derived macrophage pyroptosis in a concentration-dependent manner, and the protein expressions of p-NF- $\kappa$ B p65, NLRP3, Caspase-1, ASC, GSDMD-N, IL-1 $\beta$  and IL-18 increased significantly after treatment of the THP-1-derived macrophages with ox-LDL, compared with the NC group. Moreover, a significant increase occurred in IL-1 $\beta$  activity in the cell culture supernatant, together with an increase in the number of PI-positive cells and the LDH activity. The above data suggest that ox-LDL induced THP-1-derived macrophage pyroptosis by upregulating the NLRP3/Caspase-1 pathway, which agrees with the findings of Lin et al's study.<sup>27</sup>

The current study found that the FNDC5 overexpression in THP-1-derived macrophages caused a downregulation in the ox-LDL-induced protein expressions of p-NF- $\kappa$ B p65, NLRP3, Caspase-1, ASC, GSDMD-N, IL-1 $\beta$ , and IL-18. The IL-1 $\beta$  activity in the cell culture supernatant and the percentage of PI-positive cells and LDH activity also decreased considerably. However, silencing the FNDC5 gene only led to opposite results. The PPAR $\alpha$  protein was considerably upregulated in THP-1-derived macrophages overexpressing FNDC5.

The addition of GW6471 significantly upregulated protein expressions of p-NF- $\kappa$ B p65, NLRP3, Caspase-1, ASC, GSDMD-N, IL-1 $\beta$ , and IL-18 in the Ad-FNDC5+GW6471 group. The IL-1 $\beta$  activity in the cell culture supernatant increased noticeably. The number of PI-positive cells and LDH activity also increased. These results were consistent with those in the model group, and no significant differences existed in the above indicators ( $p > 0.05$ ). The above results suggested that FNDC5/irisin alleviated THP-1-derived macrophage pyroptosis via PPAR $\alpha$ .

## CONCLUSIONS

Irisin/PPAR $\alpha$  inhibited THP-1-derived macrophage pyroptosis and inflammation and delayed AS by inhibiting the NF- $\kappa$ B/NLRP3 pathway.

## AUTHORS' DISCLOSURE STATEMENT

The National Natural Science Foundation of China (81660083), the Scientific and Technological Innovation Talent Team Project of Guizhou Province (Qiankehe Platform Talent No. (2020)5014), and the Hundred-Level Innovative Talent Cultivation Plan Project of Guizhou Province [Qiankehe Platform Talent No. (2015)4026] supported the study. The authors have no potential conflicts of interest to report relevant to this study.

## REFERENCES

- Libby P, Buring JE, Badimon L, et al. Atherosclerosis. *Nat Rev Dis Primers*. 2019; 5(1):56. doi: 10.1038/s41572-019-0106-z
- Soehnlein O, Libby P. Targeting inflammation in atherosclerosis - From experimental insights to the clinic. *Nat Rev Drug Discov*. 2021; 20(8):589-610. doi: 10.1038/s41573-021-00198-1
- Li H, Cao Z, Wang L, et al. Macrophage subsets and death are responsible for atherosclerotic plaque formation. *Front Immunol*. 2022; 13:843712. doi: 10.3389/fimmu.2022.843712
- Zang YH, Chen D, Zhou B, et al. FNDC5 inhibits foam cell formation and monocyte adhesion in vascular smooth muscle cells via suppressing NF kappa B-mediated NLRP3 upregulation. *Vascul Pharmacol*. 2019; 121:106579. doi: 10.1016/j.vph.2019.106579
- Correa R, Silva L, Ribeiro D, et al. Lysophosphatidylcholine induces NLRP3 inflammasome-mediated foam cell formation and pyroptosis in human monocytes and endothelial cells. *Front Immunol*. 2019; 10:2927. doi: 10.3389/fimmu.2019.02927
- Xu YJ, Zheng L, Hu YW, Wang Q. Pyroptosis and its relationship to atherosclerosis. *Clin Chim Acta*. 2018; 476:28-37. doi: 10.1016/j.cca.2017.11.005
- Ding J, Wang K, Liu W, et al. Pore-forming activity and structural autoinhibition of the gasdermin family. *Nature*. 2016; 535(7610):111-116. doi: 10.1038/nature18590
- Song D, Li M, Yu X, et al. The molecular pathways of pyroptosis in atherosclerosis. *Front Cell Dev Biol*. 2022; 10(824165). doi: 10.3389/fcell.2022.824165
- Liu X, Zhang Z, Ruan J, et al. Inflammasome-activated gasdermin D causes pyroptosis by forming membrane pores. *Nature*. 2016; 535(7610):153-158. doi: 10.1038/nature18629
- Karasawa T, Takahashi M. The crystal-induced activation of NLRP3 inflammasomes in atherosclerosis. *Inflamm Regen*. 2017; 37:18. doi: 10.1186/s41232-017-0050-9
- Tabas I, Williams KJ, Boren J. Subendothelial lipoprotein retention as the initiating process in atherosclerosis: update and therapeutic implications. *Circulation*. 2007; 116(16):1832-1844. doi: 10.1161/CIRCULATIONAHA.106.676890
- Duewell P, Kono H, Rayner KJ, et al. NLRP3 inflammasomes are required for atherogenesis and activated by cholesterol crystals. *Nature*. 2010; 464(7293):1357-1361. doi: 10.1038/nature08938
- Lin J, Shou X, Mao X, et al. Oxidized low density lipoprotein induced caspase-1 mediated pyroptotic cell death in macrophages: implication in lesion instability? *Plos One*. 2013; 8(4):e62148. doi: 10.1371/journal.pone.0062148
- Pan J, Han L, Guo J, et al. AIM2 accelerates the atherosclerotic plaque progressions in ApoE-/- mice. *Biochem Biophys Res Commun*. 2018; 498(3):487-494. doi: 10.1016/j.bbrc.2018.03.005
- Xiang N, Yin T, Chen T. Gardnerella vaginalis induces NLRP3 inflammasome-mediated pyroptosis in macrophages and THP-1 monocytes. *Exp Ther Med*. 2021; 22(4):1174. doi: 10.3892/etm.2021.10609
- Shi X, Xie WL, Kong WW, Chen D, Qu P. Expression of the NLRP3 inflammasome in carotid atherosclerosis. *J Stroke Cerebrovasc Dis*. 2015; 24(11):2455-2466. doi: 10.1016/j.jstrokecerebrovasdis.2015.03.024
- Wang X, Hu Y, Wang Y, Shen D, Tao G. CLEC5A knockdown protects against cardiac dysfunction after myocardial infarction by suppressing macrophage polarization, NLRP3 inflammasome activation, and pyroptosis. *Biochem Cell Biol*. 2021; 99(5):655-665. doi: 10.1139/bcb-2020-0672
- Verma V, Gupta S, Kumar P, et al. Involvement of NLRP3 and NLR4 inflammasome in uropathogenic E. coli mediated urinary tract infections. *Front Microbiol*. 2019; 10(2020). doi: 10.3389/fmicb.2019.02020
- Bostrom P, Wu J, Jedrychowski MP, et al. A PGC1- $\alpha$ -dependent myokine that drives brown-fat-like development of white fat and thermogenesis. *Nature*. 2012; 481(7382):463-468. doi: 10.1038/nature10777
- Lin C, Guo Y, Xia Y, et al. FNDC5/Irisin attenuates diabetic cardiomyopathy in a type 2 diabetes mouse model by activation of integrin  $\alpha$ V/ $\beta$ 5-AKT signaling and reduction of oxidative/nitrosative stress. *J Mol Cell Cardiol*. 2021; 160(27-41). doi: 10.1016/j.yjmcc.2021.06.013
- Yin C, Hu W, Wang M, Lv W, Jia T, Xiao Y. Irisin as a mediator between obesity and vascular inflammation in Chinese children and adolescents. *Nutr Metab Cardiovasc Dis*. 2020; 30(2):320-329. doi: 10.1016/j.numecd.2019.09.025
- Tan J et al. The effect of irisin on atherosclerosis in apolipoprotein E gene knockout mice. *Chinese Journal of Arteriosclerosis*. 2017; 25(08):773-777.
- Wang X et al. Lentiviral vector overexpressing FNDC5 inhibits proliferation and migration of smooth muscle cells. *Chinese Journal of Tissue Engineering Research*. 2021; 25(35):5670-5675.
- He Q, Liu DN, and Tan J. Effect and mechanism of irisin on atherosclerosis in ApoE-/- mice induced by high-fat diet. *Shandong Medical Journal*, 2020; 60(22):39-43.
- Zhang Y, Song H, Zhang Y, et al. Irisin inhibits atherosclerosis by promoting endothelial proliferation through microRNA126-5p. *J Am Heart Assoc*. 2016; 5(9) doi: 10.1161/JAHA.116.004031
- Li Q, Tan Y, Chen S, et al. Irisin alleviates LPS-induced liver injury and inflammation through inhibition of NLRP3 inflammasome and NF- $\kappa$ B signaling. *J Recept Signal Transduct Res*. 2021; 41(3):294-303. doi: 10.1080/10798893.2020.1808675
- Pawlak M, Lefebvre P, Staels B. Molecular mechanism of PPAR $\alpha$  action and its impact on lipid metabolism, inflammation and fibrosis in non-alcoholic fatty liver disease. *J Hepatol*. 2015; 62(3):720-733. doi: 10.1016/j.jhep.2014.10.039
- Wu Y, Wang F, Fan L, et al. Baicalin alleviates atherosclerosis by relieving oxidative stress and inflammatory responses via inactivating the NF- $\kappa$ B and p38 MAPK signaling pathways. *Biomed Pharmacother*. 2018; 97:1673-1679. doi: 10.1016/j.biopha.2017.12.024
- Li K, Chen J, Wang C, et al. Irisin ameliorates nicotine-mediated atherosclerosis via inhibition of the PI3K pathway. *Ann Transl Med*. 2021; 9(9):805. doi: 10.21037/atm-21-2072